[*Reprinted from* THE AERONAUTICAL JOURNAL OF THE ROYAL AERONAUTICAL SOCIETY, *MAY 1993*]

The development of an efficient ornithopter wing

J. D. DELAURIER
Institute for Aerospace Studies,
University of Toronto,
Downsview, Ontario, Canada

PRINTED BY MANOR PARK PRESS LIMITED, EDISON ROAD, HAMPDEN PARK, EASTBOURNE, SUSSEX, ENGLAND
AND PUBLISHED BY THE ROYAL AERONAUTICAL SOCIETY, 4 HAMILTON PLACE, LONDON W1V 0BQ, ENGLAND

The development of an efficient ornithopter wing

J. D. DeLAURIER
Institute for Aerospace Studies,
University of Toronto,
Downsview, Ontario, Canada

ABSTRACT

Analysis and testing have been used to develop a flapping wing which can efficiently produce lift and thrust for ornithopter flight. With the assumption that the only imposed motion is dihedral flapping at its root, the wing's spanwise distribution of pitching and bending is due to its aeroelastic response. Numerical studies revealed criteria for efficient designs, which then guided the development and construction of an example wing tested in a windtunnel. The experimental results for average thrust and lift compared very favourably with the theoretical predictions, confirming that such aeroelastically tailored designs provide a means for achieving mechanical flapping-wing flight.

NOMENCLATURE

AR	Wing aspect ratio
c	Aerofoil chord
C_{hh}, $C_{h\theta}$, $C_{\theta h}$, $C_{\theta\theta}$	Structural flexibility influence coefficients
C_{mac}	Aerofoil's moment coefficient about its aerodynamic centre
C_{df}	Aerofoil's chordwise friction drag coefficient
e	Distance from leading edge to elastic axis (Fig. 2)
EI	Bending stiffness parameter at elastic axis
GJ	Torsional stiffness parameter about elastic axis
g	Gravitational constant
h	Plunging displacement of elastic axis in flapping direction
h_0	Imposed displacement of rigid spar (no bending)
$\tilde{h}$	Elastic bending relative to h_0
$\Delta\bar{h}$	Steady state elastic bending relative to h_0
δh	Time-varying elastic bending relative to steady state positions (see Equation (11))
i	Pitching moment of inertia (portion within segment width)
N	Force normal to the wing's chord
M	Pitching moment about the elastic axis
m	Mass (portion within segment width)
U	Flight speed
x_s	Distance from leading edge to spar's mass centre
y	Coordinate along the semispan
α_0	Aerofoil's zero-lift line angle with respect to its chord
α_{stall}	Aerofoil's stall angle of attack
Γ_0	Magnitude of flapping dihedral angle
η_s	Leading edge suction efficiency
θ	Pitch angle of chord with respect to U
$\bar{\theta}_a$	Pitch angle of flapping axis with respect to U
$\bar{\theta}_{wash}$	Built in pretwist angle between the chord and flapping axis for zero wind and no flapping
$\tilde{\theta}$	Elastic twist relative to the zero-wind, non-flapping, position
$\Delta\bar{\theta}$	Non-flapping elastic twist relative to zero wind position
$\delta\theta$	Time varying elastic twist relative to non-flapping position
Λ	Sweepback of elastic axis on wing's outer portion
ρ	Atmospheric density
ϕ_h	Phase angle between the bending response and the imposed motion
ϕ_θ	Phase angle between the twisting response and the imposed motion
ω	Flapping frequency, rad/sec

Subscripts

a	Apparent mass
ac	Aerodynamic centre
aero	Aerodynamic
c	Circulation
dyn	Dynamic (due to flapping)
exp	Experimental
f+r	Fabric, rib, and trailing edge
i,j	Segment indices
inertia	Inertial
static	Static (non-flapping)
theo	Theoretical

INTRODUCTION

The motivation behind this work was to invent a successful engine powered ornithopter whose flight characteristics are similar to those for large cruising birds and bats. Therefore, a specific goal for this research was to develop an efficient flapping wing which could simultaneously produce the average lift and thrust required for sustained flight.

Most previous flapping-wing designs, beginning with Alphonse Penaud's rubber powered ornithopter of 1874[1], are characterised by having a single membrane surface attached to a leading edge spar (like a traditional sail). The spar may be straight or curved back and battens or ribs may be added to give chordwise

Manuscript received 3 June 1992, accepted 22 January 1993
Paper No. 1905

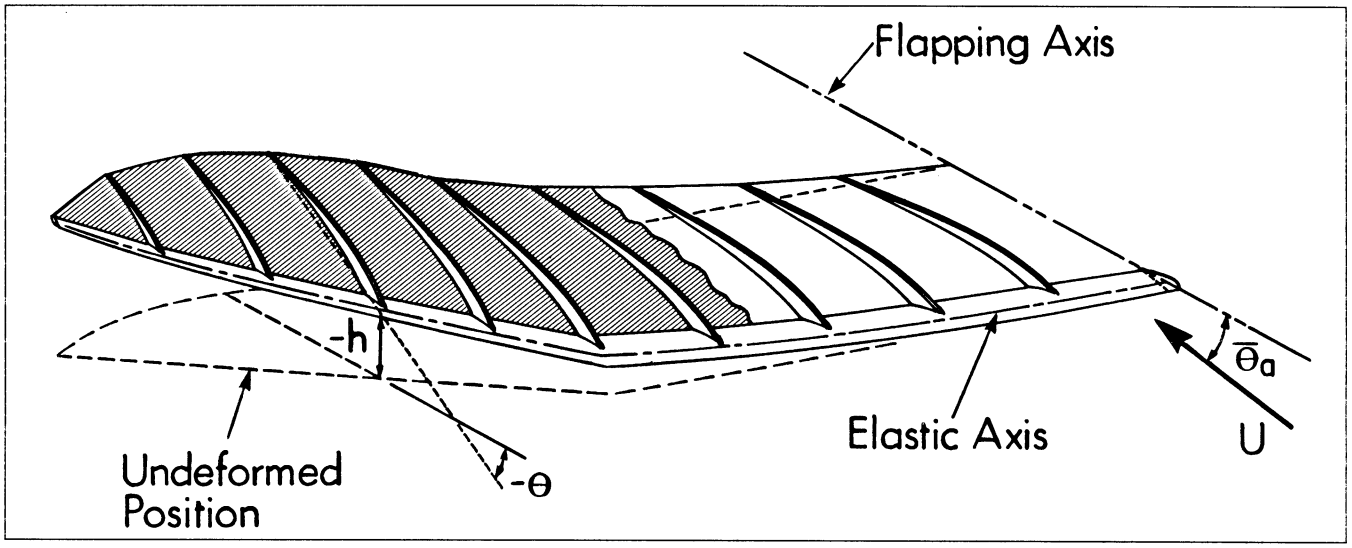

Figure 1. Wing structural deformation model.

stiffness. The wing is flapped by a periodic variation of the root dihedral angle, and the resulting aeroelastic response of the structure gives the spanwise pitching and bending distribution.

Because such wings have relatively sharp leading edges, negligible leading edge suction is produced. Therefore, the pitching action provides the thrust by giving a forward tilt to the aerofoil's normal force vector. At low advance ratios, such wings can produce significant average thrust (as described by Archer, Sapuppo, and Betteridge[2]). However, note that for a horizontal flapping axis, positive thrust on the upstroke corresponds to negative lift, and positive lift on the upstroke generally implies negative thrust (modified only slightly by the presence of any fixed camber).

Rayner[3] describes how birds and bats, which also have low leading edge suction, compensate for this by varying their semispan length between upstroke and downstroke. Ornithopter designers, though, have preferred to avoid this additional mechanical complication. Instead, the usual approach has been to utilise a membrane wing designed to give positive thrust on both upstroke and downstroke, and then trim the aircraft to fly at a fairly high angle so that the thrust vector gives a significant lift component. The balance of the required lift is then given by various fixed surfaces on the aircraft. Although this has been successful for numerous small rubber powered ornithopters, the propulsive efficiency is quite poor and it was not considered to be very promising for a larger engine powered aircraft.

A different approach was taken by AeroVironment for a 18 ft span mechanical flying pterosaur replica (Project QN)[4]. By means of an elastic covering it was possible to incorporate a double-surface aerofoil and still maintain twisting ability. Also, this twisting was mechanically imposed so that the wing motions for maximum propulsive efficiency (derived by Ilan Kroo in Ref. 4) could be directly achieved. However, this wing was not optimised for ornithopter flight, *per se*. The configuration and surface texture were largely defined by paleontological evidence and, as described in Ref. 5, this requirement for biological realism resulted in an efficiency compromise.

For the present development, it was desired to retain the Penaud wing's mechanical simplicity of imposing motion only at the root dihedral angle and allowing the aeroelastic response to determine the twist distribution. The wing is also assumed to maintain a constant semispan throughout the flapping cycle; however, a special design feature allows chordwise-rigid, double-surface aerofoils with high leading edge suction to be incorporated into a torsionally compliant structure. Therefore, efficient mean thrusting and lifting are simultaneously produced at high advance ratios and flapping-axis angles near horizontal. An aeroelastic analysis is used to obtain the wing's pitching and bending behaviour, and the results are coupled with the aerodynamic model described in Ref. 5 to predict the wing's performance.

METHOD OF ANALYSIS

The structural model for the wing is represented in Fig. 1, where it is seen to consist of a single leading edge spar to which chordwise ribs are firmly attached. The continuous elastic axis of the spar consists of two straight portions: one which extends, unswept, from the flapping axis to a sharp bend ("crank"); and one which, beyond the crank, has a uniform sweep in the chordwise direction. The spar can bend and twist as shown, but the ribs are assumed to be chordwise rigid.

The wing's bending displacement is measured by coordinate $h(y)$, which is perpendicular to the flapping axis; and its twist is measured by an angular coordinate $\theta(y)$, which is in the plane of $h(y)$ and the flapping axis. For analytical convenience, the wing will be divided into n discrete segments, with $h(y)$ and $\theta(y)$ replaced by h_i and θ_i, where station i is chosen to be the midpoint of the segments. Therefore, the wing's coordinates are given by the column vectors:

$$\{\mathbf{h}\} \text{ and } \{\theta\} \qquad \ldots (1)$$

Further, the spar is assumed to have an imposed time-varying displacement, $\{\mathbf{h_0}\}$, from mechanical forcing, so that

$$\{\mathbf{h}\} = \{\mathbf{h_0}\} + \{\tilde{\mathbf{h}}\} \qquad \ldots (2)$$

where $\{\tilde{\mathbf{h}}\}$ is the elastic displacement. Likewise, $\{\theta\}$ is assumed to consist of the flapping-axis angle, $\bar{\theta}_a$, a built in pretwist distribution, $\{\bar{\theta}_{\mathbf{wash}}\}$, and an elastic component, $\{\tilde{\theta}\}$:

$$\{\theta\} = \bar{\theta}_a + \{\bar{\theta}_{\mathbf{wash}}\} + \{\tilde{\theta}\} \qquad \ldots (3)$$

Now, the loads at each segment consist of a force, N_i, normal to the chord and a pitching moment, M_i, about the elastic axis, where M_i has the same sense and orientation as θ_i. Therefore, the loads and elastic deformations are related through a $2n \times 2n$ matrix of structural flexibility influence coefficients:

$$\begin{bmatrix} [\mathbf{C_{hh}}] & [\mathbf{C_{h\theta}}] \\ [\mathbf{C_{\theta h}}] & [\mathbf{C_{\theta\theta}}] \end{bmatrix} \begin{Bmatrix} -\{\mathbf{N}\} \\ \{\mathbf{M}\} \end{Bmatrix} = \begin{Bmatrix} \{\tilde{\mathbf{h}}\} \\ \{\tilde{\theta}\} \end{Bmatrix} \qquad \ldots (4)$$

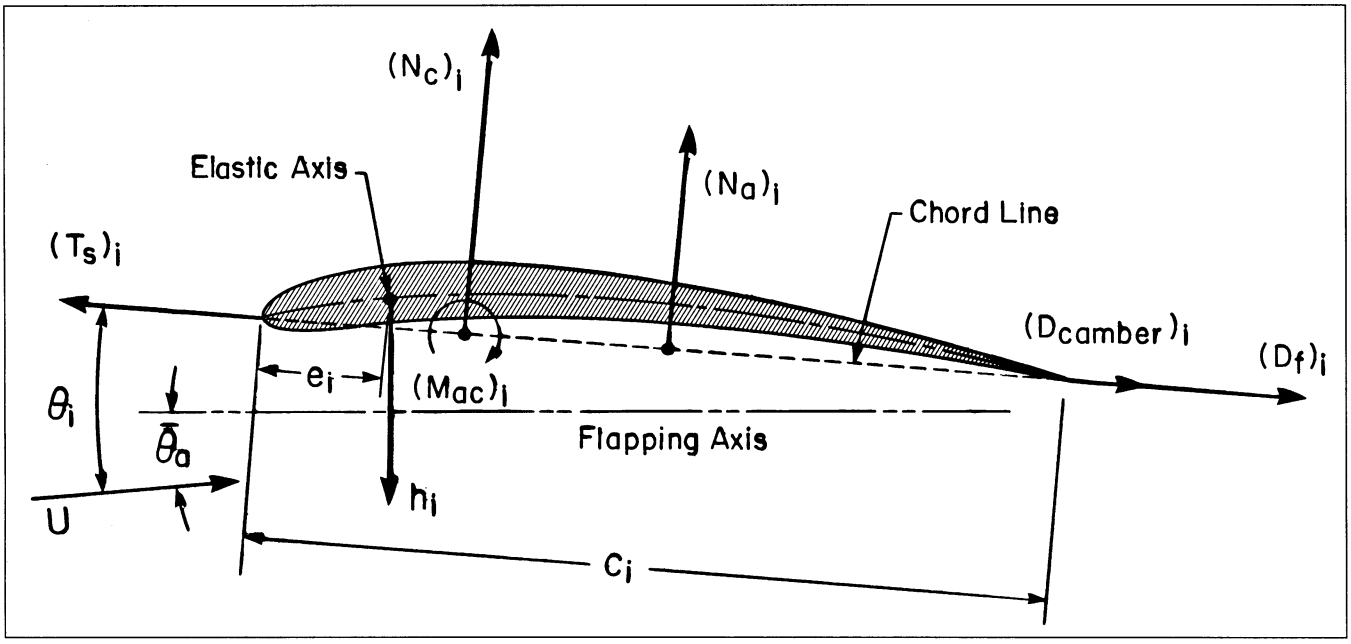

Figure 2. Aerodynamic loads on wing segment.

where the off-diagonal submatrices $[\mathbf{C}_{h\theta}]$ and $[\mathbf{C}_{\theta h}]$ are due to the crank in the spar's elastic axis. Note that the elements of these matrices are related by

$$(C_{h\theta})_{i,j} = (C_{\theta h})_{j,i} \quad \ldots (5)$$

Also, these values are zero for stations i and j inboard of the crank.

The load matrices $\{\mathbf{N}\}$ and $\{\mathbf{M}\}$ are composed of aerodynamic and inertial-reaction forces and moments. The segment's aerodynamic loads are represented in Fig. 2 (for completeness, the chordwise forces are also shown although, to first order, they make no contribution to the load matrices). From this, one sees that the segment's aerodynamic normal force is

$$(N_{aero})_i = (N_c)_i + (N_a)_i \quad \ldots (6)$$

and the moment about its elastic axis is

$$(M_{aero})_i = (M_{ac})_i - (N_c)_i(0\cdot 25c_i - e_i) - (N_a)_i(0\cdot 5c_i - e_i) \quad \ldots (7)$$

where $(N_c)_i$ is the normal force due to circulation,

$$(N_c)_i = (C_n)_i \frac{\rho U^2}{2} c_i \Delta y_i \quad \ldots (8)$$

$(N_a)_i$ is the normal force due to apparent mass,

$$(N_a)_i = 0\cdot 25\rho\pi c_i^2 (\dot{v}_2)_i \Delta y_i \quad \ldots (9)$$

and $(M_{ac})_i$ is the moment about the aerodynamic centre,

$$(M_{ac})_i = \left(C_{m_{ac}}\right)_i \frac{\rho U^2}{2} c_i^2 \Delta y_i \quad \ldots (10)$$

The expressions for the circulation normal-force coefficient, $(C_n)_i$, and the midchord normal velocity, $(v_2)_i$, are given in Ref. 5, where it is seen that they are functions of θ_i and the time derivatives of h_i and θ_i.

Further, note that the elastic deformations consist of mean values plus unsteady parts:

$$\begin{aligned} \tilde{h}_i &= \Delta\bar{h}_i + \delta h_i \\ \tilde{\theta}_i &= \Delta\bar{\theta}_i + \delta\theta_i \end{aligned} \quad \ldots (11)$$

The mean values, $\Delta\bar{h}_i$ and $\Delta\bar{\theta}_i$, are the non-flapping elastic deformations, relative to the zero wind configuration; and the unsteady values, δh_i and $\delta\theta_i$, are the time varying elastic deformations relative to the mean values.

The inertial-reaction loads are represented in Fig. 3, where it is seen that the segment's mass components consist of the spar and the $f + r$ (fabric, ribs, and trailing edge) surface. The masses of the ribs and trailing edge are averaged over the segment's area, $c_i \times \Delta y_i$, and added to the fabric's mass to give a uniform surface, the mass centre of which is at the segment's midchord. Therefore, the total inertial-reaction force is:

$$\begin{aligned} (N_{inertia})_i = &\left[(m_{f+r})_i + (m_{spar})_i\right]\left[(\ddot{h}_0)_i + \delta\ddot{h}_i - g\right] \\ &+\left[(m_{f+r})_i(0\cdot 5c_i - e_i) + (m_{spar})_i(x_{s_i} - e_i)\right]\delta\ddot{\theta}_i \end{aligned} \quad \ldots (12)$$

and the inertial-reaction moment about the segment's elastic axis is:

$$\begin{aligned} (M_{inertia})_i = &\left[(0\cdot 5c_i - e_i)(m_{f+r})_i + (x_{s_i} - e_i)(m_{spar})_i\right]\left[g - (\ddot{h}_0)_i - \delta\ddot{h}_i\right] \\ &-\left[(0\cdot 5c_i - e_i)^2(m_{f+r})_i + (x_{s_i} - e_i)^2(m_{spar})_i\right]\delta\ddot{\theta}_i \\ &-\left[(i_{f+r})_i + (i_{spar})_i\right]\delta\ddot{\theta}_i \end{aligned} \quad \ldots (13)$$

The inertial loads may be added to the aerodynamic loads to give the total normal force and moment applied to the segment:

$$\begin{aligned} N_i &= (N_{aero})_i + (N_{inertia})_i \\ M_i &= (M_{aero})_i + (M_{inertia})_i \end{aligned} \quad \ldots (14)$$

When Equations (5), (6), (10), and (11) are substituted into Equation (12), one finds that the total loads may be written as:

$$\begin{aligned} N_i &= (N_{static})_i + (N_{dyn})_i \\ M_i &= (M_{static})_i + (M_{dyn})_i \end{aligned} \quad \ldots (15)$$

where the static terms are linear functions of $\bar{\theta}_a$, $(\bar{\theta}_{wash})_i$ and $\Delta\bar{\theta}_i$; and the dynamic terms are linear functions of $\delta\theta_i$ and the time derivatives of $(h_0)_i$, δh_i, and $\delta\theta_i$. Therefore, $(N_{static})_i$ and $(M_{static})_i$ are the aerodynamic and gravity loads on the non-flapping wing; and $(N_{dyn})_i$ and $(M_{dyn})_i$ are the aerodynamic and inertial loads generated by the wing's motion.

When Equations (15) are substituted into Equation (3), the problem separates into two sets of linear equations, one for the

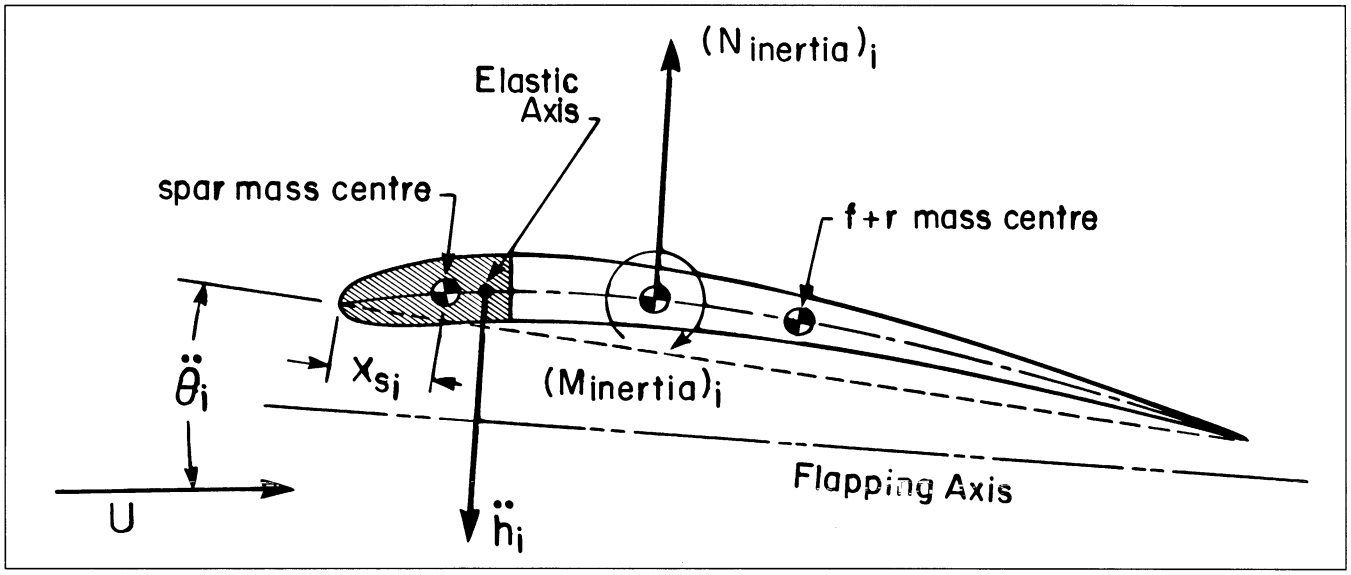

Figure 3. Inertial loads on wing segment.

static deformation, and another for the dynamic response. The static equations become:

$$\begin{bmatrix}[\mathbf{A}_{1,1}] & [\mathbf{A}_{1,2}]\\ [\mathbf{A}_{2,1}] & [\mathbf{A}_{2,2}]\end{bmatrix}\begin{Bmatrix}\{\Delta\bar{\theta}\}\\ \{\Delta\bar{\theta}\}\end{Bmatrix}-\begin{Bmatrix}\{\Delta\bar{h}\}\\ \{\Delta\bar{\theta}\}\end{Bmatrix}=\begin{Bmatrix}\{\mathbf{B}_1\}\\ \{\mathbf{B}_2\}\end{Bmatrix} \quad \ldots(16)$$

where matrices **[A]** and **{B}** incorporate the structural influence coefficients and coefficients from the equations for $(N_{static})_i$ and $(M_{static})_i$. Also, note that **{B}** are functions of $\bar{\theta}_a$ and $(\bar{\theta}_{wash})_i$.

The equations, when expanded out, uncouple into two distinct problems:

$$\left[[\mathbf{A}_{1,1}]+[\mathbf{A}_{1,2}]\right]\{\Delta\bar{\theta}\}-\{\Delta\bar{\mathbf{h}}\}=\{\mathbf{B}_1\} \quad \ldots(17)$$

$$\left[[\mathbf{A}_{2,1}]+[\mathbf{A}_{2,2}]-[\mathbf{I}]\right]\{\Delta\bar{\theta}\}=\{\mathbf{B}_2\} \quad \ldots(18)$$

where **[I]** is the identity matrix. A solution for $\{\Delta\bar{\theta}\}$ may be obtained from Equation (18), and this value is substituted into Equation (17) to find $\{\Delta\bar{\mathbf{h}}\}$. Therefore, the wing's static twist distribution, relative to the flapping-axis, is obtained from Equations (3) and (11) as

$$\{\bar{\theta}_w\}=\{\bar{\theta}_{wash}\}+\{\Delta\bar{\theta}\} \quad \ldots(19)$$

Further, Equations (2) and (11) show that $\{\Delta\bar{\mathbf{h}}\}$ is the elastic axis' static bending distribution under the aerodynamic and gravitational loads.

The equations for the dynamic variables, δh and $\delta\theta$, become:

$$-\begin{bmatrix}[\mathbf{E}_1] & [\mathbf{0}]\\ [\mathbf{E}_2] & [\mathbf{0}]\end{bmatrix}\begin{Bmatrix}\{\ddot{\mathbf{h}}_0\}\\ \{\mathbf{0}\}\end{Bmatrix}-\begin{bmatrix}[\mathbf{F}_1] & [\mathbf{0}]\\ [\mathbf{F}_2] & [\mathbf{0}]\end{bmatrix}\begin{Bmatrix}\{\dot{\mathbf{h}}_0\}\\ \{\mathbf{0}\}\end{Bmatrix}=$$
$$\begin{bmatrix}[\mathbf{E}_1] & [\mathbf{G}_1]\\ [\mathbf{E}_2] & [\mathbf{G}_2]\end{bmatrix}\begin{Bmatrix}\{\delta\ddot{\mathbf{h}}\}\\ \{\delta\ddot{\theta}\}\end{Bmatrix}+\begin{bmatrix}[\mathbf{F}_1] & [\mathbf{H}_1]\\ [\mathbf{F}_2] & [\mathbf{H}_2]\end{bmatrix}\begin{Bmatrix}\{\delta\dot{\mathbf{h}}\}\\ \{\delta\dot{\theta}\}\end{Bmatrix} \quad \ldots(20)$$
$$+\begin{bmatrix}[-\mathbf{I}] & [\mathbf{J}_1]\\ [\mathbf{0}] & [\mathbf{J}_2-\mathbf{I}]\end{bmatrix}\begin{Bmatrix}\{\delta\mathbf{h}\}\\ \{\delta\theta\}\end{Bmatrix}$$

where the matrices **[E]**, **[F]**, **[G]**, **[H]**, and **[J]** incorporate the structural influence coefficients and coefficients from the equations for $(N_{dyn})_i$ and $(M_{dyn})_i$. The solution for these is found by assuming, first, that the imposed displacement, $\{\mathbf{h_0}\}$, has a simple harmonic motion:

$$(h_0)_i=(H_0)_i e^{i\omega t} \quad \ldots(21)$$

therefore, δh_i and $\delta\theta_i$ have a steady state response given by

$$\delta h_i=H_i e^{i\omega t}, \qquad \delta\theta_i=\Theta_i e^{i\omega t} \quad \ldots(22)$$

H_i and Θ_i are, in general, complex, which gives the phase differences along the span relative to the imposed motion, $(h_0)_i$. When Equations (22) are substituted into Equations (20), a $2\times n$ system of complex linear equations are obtained for H_i and Θ_i. Further, these may be separated into real and imaginary parts, so that a $4\times n$ system of real linear equations is obtained for $(H_{real})_i$, $(H_{imag})_i$, $(\Theta_{real})_i$, and $(\Theta_{imag})_i$. Upon solving for these variables and choosing the real parts of Equations (22), one obtains that:

$$\begin{aligned}\delta h_i&=\bar{H}_i\mathrm{Cos}\left[\omega t+(\phi_h)_i\right]\\ \delta\theta_i&=\bar{\Theta}_i\mathrm{Cos}\left[\omega t+(\phi_\theta)_i\right]\end{aligned} \quad \ldots(23)$$

where

$$\begin{aligned}\bar{H}_i&=\left(H_{real}^2+H_{imag}^2\right)^{\frac{1}{2}}\\ \bar{\Theta}_i&=\left(\Theta_{real}^2+\Theta_{imag}^2\right)^{\frac{1}{2}}\end{aligned} \quad \ldots(24)$$

and

$$\begin{aligned}(\phi_h)_i&=\mathrm{Tan}^{-1}\left(\frac{H_{imag}}{H_{real}}\right)\\ (\phi_\theta)_i&=\mathrm{Tan}^{-1}\left(\frac{\Theta_{imag}}{\Theta_{real}}\right)\end{aligned} \quad \ldots(25)$$

Note that these responses are due to an $(h_0)_i$ given by the real part of Equation (21):

$$(h_0)_i=(H_0)_i\mathrm{Cos}(\omega t) \quad \ldots(26)$$

Equations (19) and (23) give the deformation and motion parameters necessary for calculating the wing's performance from the aerodynamic equations in Ref. (5). As stated before, equations from the same reference were used for obtaining $(N_{aero})_i$ and $(M_{aero})_i$. However, there are two important differences. First, the freestream dynamic pressure was used in Equations (8) and (10) instead of the local dynamic pressure at the segment's 1/4 chord location (which includes the flapping velocities as well as U).

Second, no stalling was allowed. These assumptions were necessary in order to obtain linear equations for the deformation and motion parameters. In practice, these are reasonable in that, for the type of fast cruising flight being studied, the local dynamic pressure is within a few percent of the freestream value. Also,

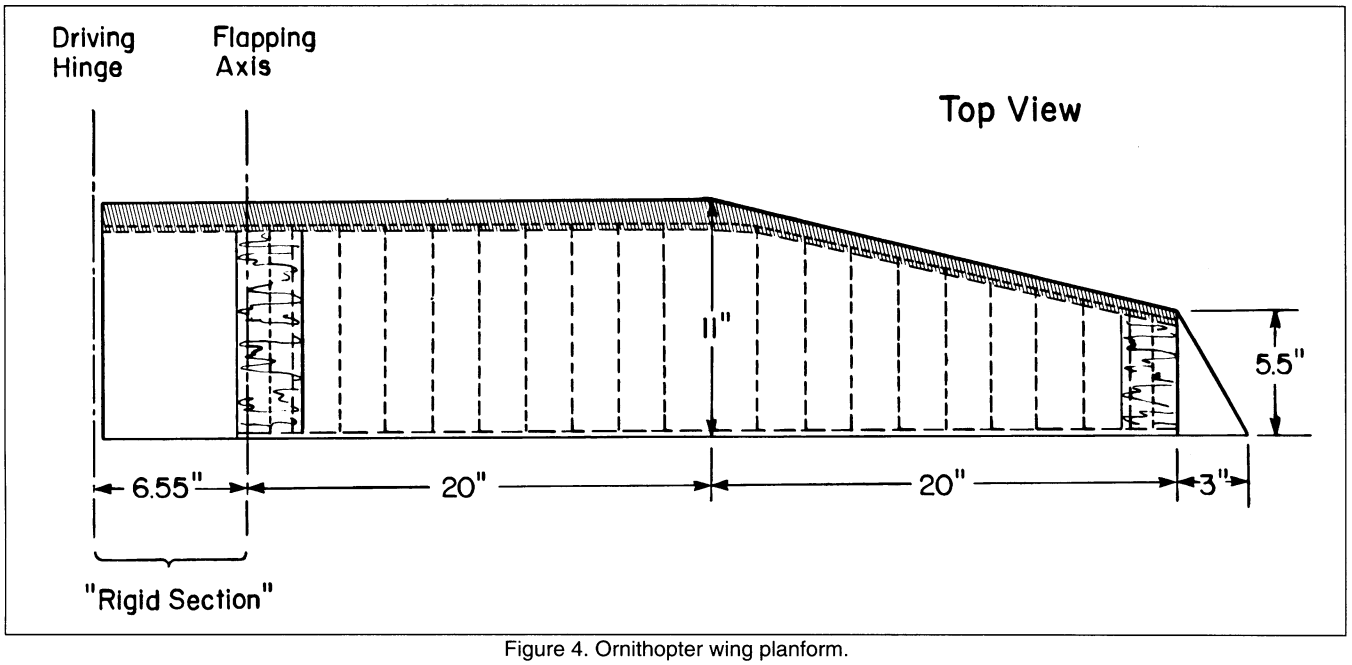

Figure 4. Ornithopter wing planform.

efficient flapping has limited stalling, so when the analysis is applied to such a wing (by design iteration), the no-stall assumption is largely satisfied.

However, for the performance calculations there is no reason not to take advantage of the greater accuracy offered by the equations in Ref. (5). Therefore, the pitching and bending analysis from above was combined with the performance analysis of Ref. (5) to give a means for the iterative design of an efficient flapping wing. The resulting program was named "ComboWing", and its application to a candidate ornithopter wing is now described.

APPLICATION TO WING DESIGN

General criteria

ComboWing was used to analyse a sequence of wing designs which evolved to the one described in this article. Space does not permit a detailed description of this evolution, but it should be mentioned that several important design features became evident early in this study. First, as described in Ref. (5), efficient flapping is characterised by pitching angles lagging plunging displacements by $\approx 90°$. The aerodynamic loads, alone, act to give that phasing if the aerodynamic centres are located aft of the elastic axis (as shown in Fig. 2). Therefore, the wings are designed with the spar as far forward within the aerofoil's profile as possible, yet still having adequate dimensions for strength. Further, the fabric, ribs, and trailing edge should have negligible spanwise bending stiffness so that the wing's elastic axis is the same as the spar's.

The second design feature is the cranked spar, shown in Fig. 1. This serves to increase the distance between the pressure centres on the outer portion and the elastic axis on the inner portion, thus increasing the twisting action without changing the spar's torsional stiffness. The sweep angle, Λ, therefore becomes a useful design variable for achieving a desired pitch-distribution response. It is interesting that this is also a feature on most bird and bat wings.

Third, it was found that the $f + r$ (fabric, ribs, and trailing edge) mass should be kept as low as possible. Mass located aft of the elastic axis tends to drive the phasing towards 180°, which dramatically reduces the wing's performance. Therefore, very light construction is required aft of the spar.

Fourth, although the spar has to have a certain torsional compliance in order to give the required twisting, it was found that too much bending compliance could also give inefficient phasing between pitching and plunging. Thus the spar has to be designed to give significant bending stiffness as well as torsional flexibility.

Finally, besides being light and giving no bending resistance, the covering is also required to give very little torsional resistance and present a reasonably smooth aerodynamic surface. This was initially accomplished by using a single-surface design, as shown in Fig. 1. However, even with a faired leading edge, single-surface aerofoils have a much poorer angle of attack range for attached flow than a well designed double-surface section (as described in Ref. 6). Further, the double-surface aerofoil has a much higher leading edge suction efficiency. This gave a very strong motivation to use double-surface sections. The problem was that in covering such an aerofoil, the closed cross sectional envelope could give significant torsional resistance, wrinkling considerably in the process.

One solution would have been to use a compliant skin, such as latex. However, all materials considered had such excessive mass that inefficient phasing between pitching and plunging would have occurred, as described previously. Another solution was invented by the author and his co-investigator, Jeremy Harris. This is called "Shearflexing", and entails splitting the trailing edge so that the upper and lower surfaces have relative spanwise freedom. That is, the double-surface wing is considered to be composed of two superimposed single-surface wings joined at the spar. With this, large twisting deflections are readily achieved in response to the imposed loads.

Specific wing design

As mentioned in the Introduction, this work was directed towards the wing design for a specific ornithopter. The design which evolved from the performance requirements and the above considerations is illustrated in Figs 4 and 5. Structurally, this consists of a composite spar to which reinforced foam ribs are attached. Two unidirectional carbon fibre/epoxy strips are glued to the ends of the ribs to form the trailing edge. However, these are not glued to

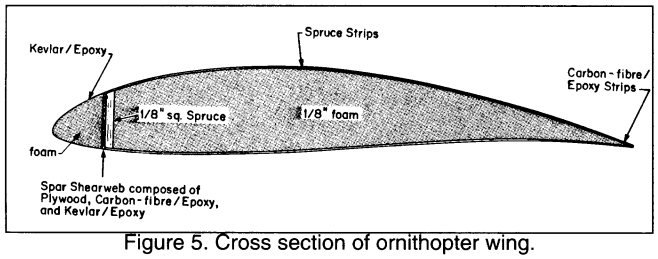

Figure 5. Cross section of ornithopter wing.

each other. Instead, clips are attached which prevent spreading of the trailing edge while allowing free relative lateral motion between the strips. This permits the Shearflexing action to occur, as illustrated in Fig. 6. Also, the covering is required to be attached to alternating ribs, as shown.

It should be noted that Shearflexing can work with solid skin wings as well as the presently discussed fabric covered wing. The essential feature is that the trailing edge has to be split, thus opening the "torque box" formed by the aerofoil's cross section. There are still some shearing stresses in the skins which can give rise to stress wrinkles in the fabric covering. However, these have not been found to be aerodynamically excessive, and pretensioning of the covering largely eliminates these during most of the flapping cycle.

The spar was designed to have certain required elastic properties. First, the high bending stiffness (characterised by *EI*) was produced by a full depth plywood shear web faced with spanwise-directional carbon fibre/epoxy sheet, as shown in Fig. 5. Next, the torsional cross section is constructed by attaching foam blocks to the shear web, cutting these to the aerofoil's leading edge shape, and covering with epoxy-impregnated Kevlar cloth with the warp fibres orientated parallel to the elastic axis. The number of layers and the dimensions of the spar determine the resulting torsional stiffness (characterised by *GJ*). Stiffness tests on various sample spars gave *GJ* and *EI* values which could be scaled for the wing's design. It was found that, for a given shear web and Kevlar skin thickness, the scaling varied approximately as the third power of the shear web height.

The Shearflexing action requires the twisting to vary linearly with span. Additionally, ComboWing showed linear twisting to be desirable for efficient flapping. Therefore, the *GJ* distribution had to be tailored to give this as well as producing the correct magnitudes. As determined by numerical iteration, the required *GJ* distribution for the wing is shown in Fig. 7. It should be noted that aerodynamic help was also needed from the rigid delta shaped wing tip in order to give linear twisting out to the end.

The *GJ* values, along with the wing's other parameters, are tabulated in the Appendix. Special note should be made of the aerofoils' excellent aerodynamic characteristics. The section

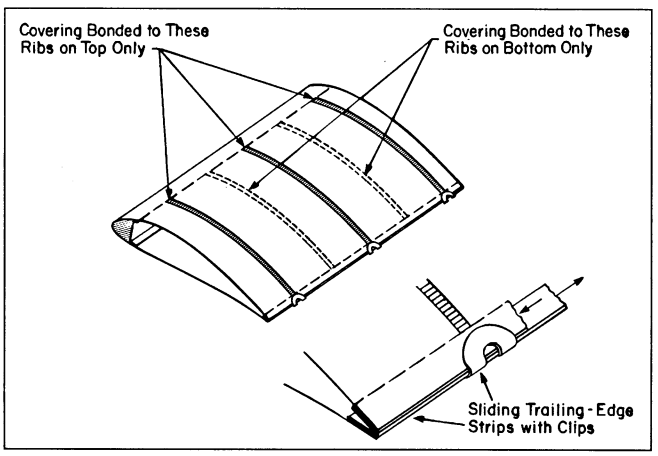

Figure 6. Structural design for Shearflexing

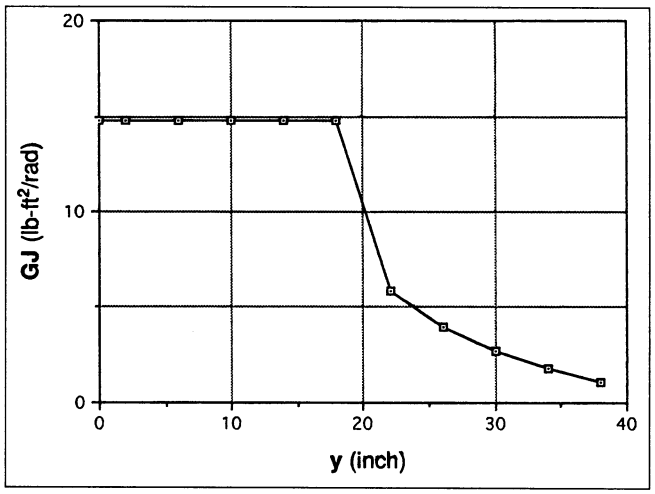

Figure 7. Torsional stiffness distribution.

along the constant chord portion, named S1020, is shown in Fig. 5. This was especially designed for the ornithopter project, by Michael Selig of the Pennsylvania State University, to have a wide attached flow angle of attack range along with a high leading edge suction efficiency (for the RN of 2×10^5). Windtunnel tests confirmed Selig's theoretical predictions. Also, note the structural bonus of having a deep and full leading edge shape. On the wing's tapered portion, the S1020 aerofoil varies its shape linearly to a symmetrical, Selig and Donovan SD8020, section at the tip.

The version of ComboWing used to predict the wing's performance assumed that the imposed plunging, $\{\mathbf{h_0}\}$, was linear from the flapping axis to the tip. Therefore, from Equation (26), $(H_0)_i$ is given by

$$(H_0)_i = y_i \mathrm{Sin}\Gamma_0 \qquad \ldots (27)$$

Also, the wing was assumed to be cantilevered relative to the imposed motion at the flapping axis, thus the structural influence coefficients are calculated for such a beam.

Calculated performance

The wing's required lift was determined by the ornithopter's weight, and a drag test of the ornithopter minus its wing gave the thrust value needed for equilibrium flight. It was found that the wing achieved this performance at a speed of 45 ft/sec and a flapping-axis angle, $\bar{\theta}_a$, of 6° where, for a flapping frequency of 2·4 Hz, the single-panel average lift was 4·3 lb and the average thrust was 0·24 lb. Further, the average propulsive efficiency for this condition was calculated to be 50%. As discussed in Ref. 5, this may seem low in comparison with propeller efficiencies (which are typically above 80%); but it should be noted that the definition for flapping-wing propulsive efficiency incorporates the wing's drag, including that due to its mean lift. Therefore, 50% actually denotes a very efficient thruster.

Some flow separation was predicted on the outer 12 in (excluding the delta tip) during midstroke portions of the cycle. It was found that if the wing was allowed to twist sufficiently to prevent separation, its overall performance would be greatly reduced. As discussed in Ref. 5, efficient flapping by this type of rigid semispan wing seems to necessitate a certain amount of separation during the cycle. However, it should be noted that if, for the same amount of twisting, no separation occurred, there would be a small increase in performance.

The calculated values of the dynamic-response twisting and bending are shown in Fig. 8. The twisting magnitude variation is seen to be fairly linear, in accordance with the *GJ* distribution previously discussed. Also, the phase angles for twisting are close to the desired values of –90°. The shape for the bending response is typical of that for a cantilevered beam, with a tip displacement of

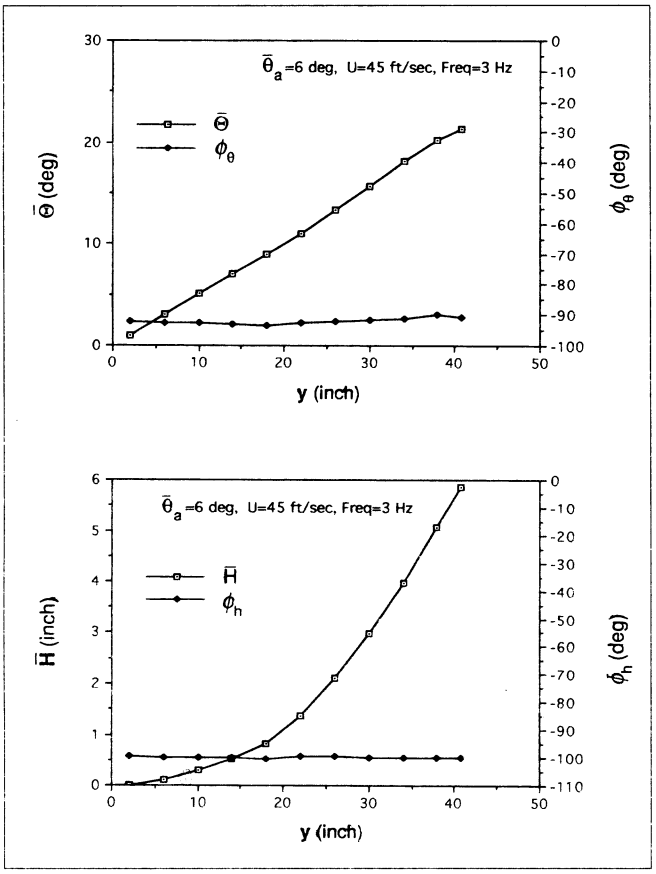

Figure 8. Dynamic-response distributions.

less than 6 in occurring approximately at mid-downstroke and mid-upstroke. Therefore, contributions from modal resonances appear to be minimal.

A maximum bending moment of 12·2 ftlb at the flapping axis was predicted. In comparison with breaking tests on the spar samples, this gave a safety factor of 3. The bending moment value also allowed a calculation of the peak power required during the flapping cycle. It was found that this was within the engine's 1 hp capability by a factor of 2 (based on two wing panels).

Finally, Fig. 9 shows the behaviour, during the flapping cycle, of a 4 in wide segment whose midpoint is 30 in from the flapping axis (Segment 8 in the Appendix). Although both negative and positive lift is generated, the average lift has the required positive value. Also, this diagram clearly shows how the leading edge suction gives positive thrust nearly throughout the cycle.

EXPERIMENTAL COMPARISON AND DISCUSSION OF RESULTS

The wing was mounted on a special flapping rig in the Institute for Aerospace Studies' subsonic wind tunnel in order to measure its performance and provide data for comparison with the Combo-Wing predictions. The flapping rig was designed and built by William McKinney and Henry Kwok, graduate engineers at the Institute. This was a challenging research project in itself, worthy of being described in a separate article. Briefly, however, the rig consists of a rigid frame, mounted to the top of the wind tunnel, from which a horizontal platform is suspended by four thin wires. Therefore, the platform can translate horizontally just above the top of the wind tunnel. This movement is restrained, and the corresponding reaction forces measured, by three strain gauge balances located at the edges and connected to the frame.

The flapping motor and drive reduction are mounted on the platform, as well as the wing's flapping-axis hinge. Therefore, the wing extends through holes in the platform and the top of the tunnel into the test section. The flapping is driven at the platform, with the major portion of the wing being in the windtunnel's air flow, as shown in Fig. 10. It is also seen that in order to provide an aerodynamic boundary where the wing enters the windtunnel, an aluminum plate is suspended from the platform. This has a cutout for the wing to pass through, and the seal is completed with "Dental Dam" latex rubber taped to stretch from the cutout to the wing. Note that the plate is not directly attached to the wind tunnel, therefore the latex seal does not influence the balance readings.

The readings are digitised and averaged over a time interval, which eliminates the unbalanced inertial-reaction forces caused by

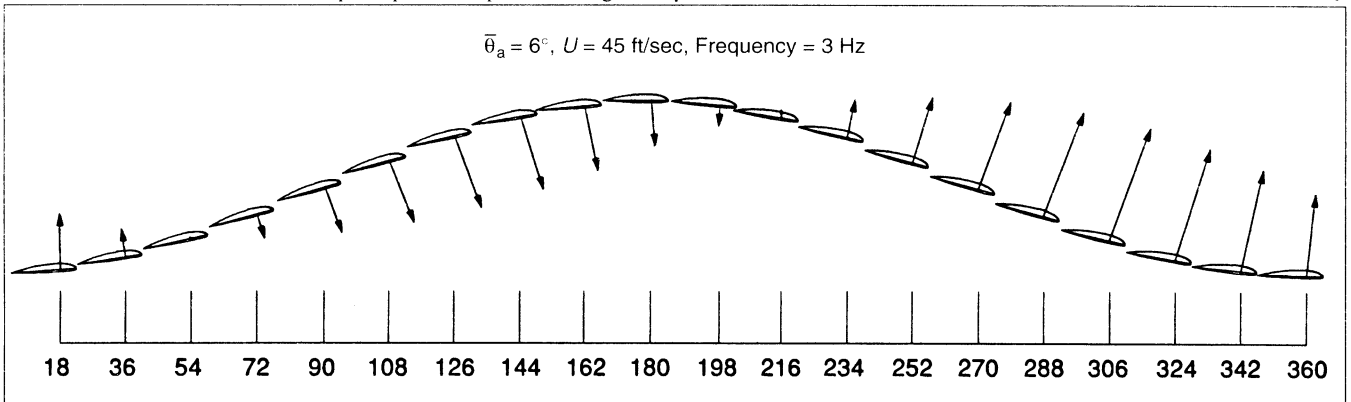

Force scaling: Maximum net force (306°) = 0·824 lb

Maximum segment thrust (306°) = 0·280 lb
Maximum segment lift (306°) = 0·775 lb
Average segment thrust = 0·107 lb

Average segment lift = 0·133 lb
Segment span = 4·0 in
Segment chord = 8.25 in

Figure 9. Cycle history of segment 8.

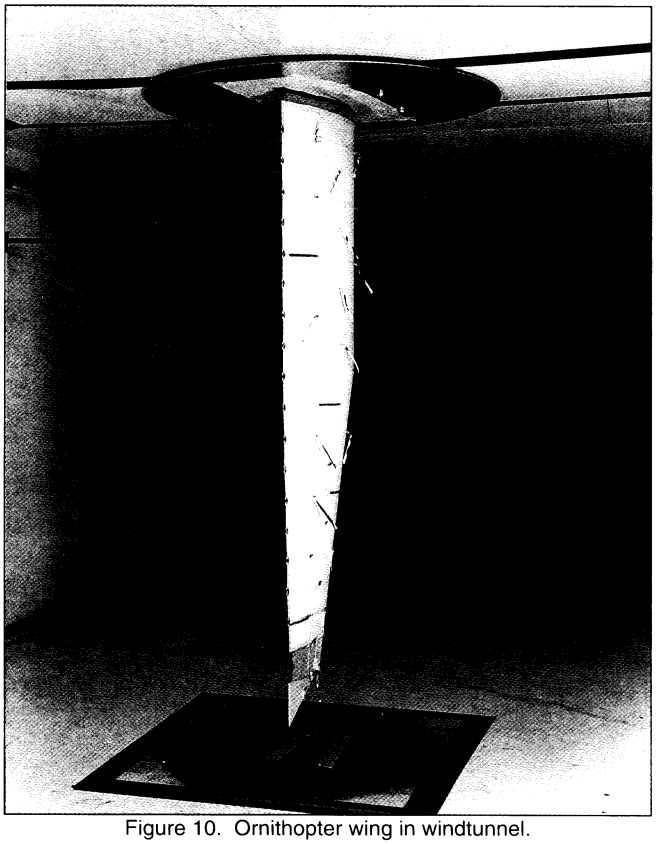

Figure 10. Ornithopter wing in windtunnel.

the flapping. With the three balances, average thrust, lift, and pitching moment were obtained. The results for thrust and lift *vs* flapping frequency are shown for the candidate wing in Fig. 11. Also plotted are the ComboWing predictions, where it is seen that the comparison is quite favourable. It should be stated that the results shown in Fig. 11 are very representative of a large number of experimental comparisons for this wing at different speed and angle conditions, and for several repeats. In all cases, ComboWing predicts somewhat better lift and thrust performance, although the experimental results are still within the ornithopter's flight requirements.

It was speculated that, despite the end plate, there was an aerodynamic degradation caused by the opening through the top of the windtunnel's test section. This was assessed by, first, measuring zero frequency ("static") values with a cardboard mask fitted close (1/8 in gap) to the wing and taped to the windtunnel ceiling (only possible for zero flapping). Next, the mask was replaced by the plate assembly, and values were obtained with and without the dental dam seal. It was found that the sealed gap gave a significant increase of lift and decrease of drag, and that the values were virtually identical to those for the masked case. Therefore, the plate and seal were judged to be at least as effective as the mask in giving an aerodynamic boundary (image plane) at the root.

Another static measurement was the wing's tip deflection. Figure 10 shows the plexiglass window, in the windtunnel floor, through which these values were obtained by marking the tip's wind on and wind off positions. For the U = 45ft/sec and $\bar{\theta}_a = 6°$ case, it was found that

$$\left(\Delta\bar{\theta}_{tip}\right)_{exp} = -9\cdot0^{\circ}$$

$$\left(\Delta\bar{h}_{tip}\right)_{exp} = -1\cdot38\,\text{in}$$

which compare with the ComboWing-predicted values of

$$\left(\Delta\bar{\theta}_{tip}\right)_{theo} = -8\cdot1^{\circ}$$

$$\left(\Delta\bar{h}_{tip}\right)_{theo} = -1\cdot58\,\text{in}$$

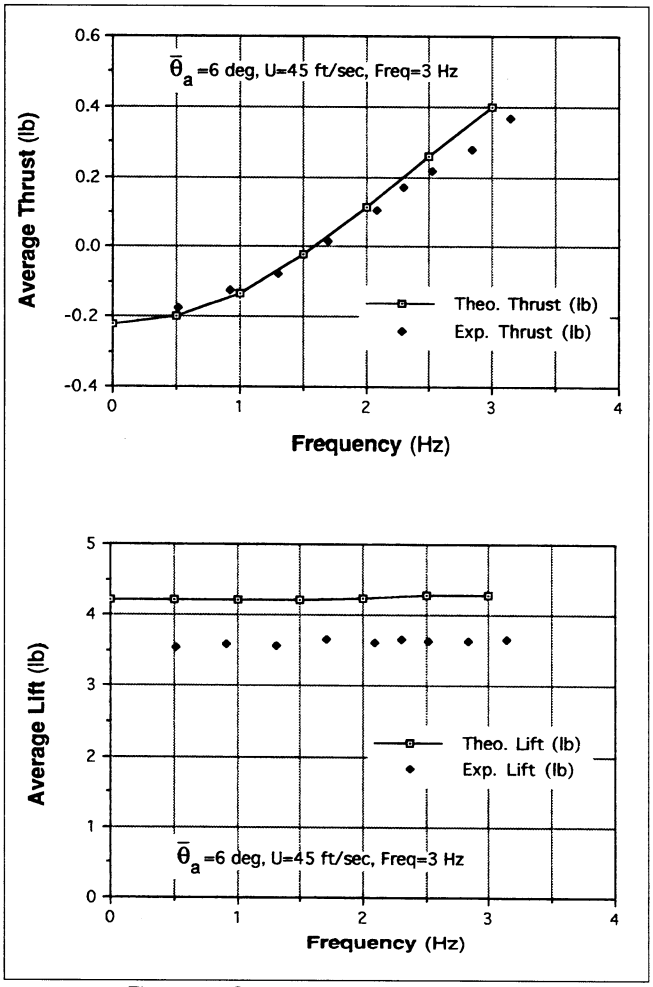

Figure 11. Ornithopter wing performance.

Again, this is a favourable comparison considering the numerous assumptions in the physical model and unavoidable differences between the estimated and as-built values for certain parameters (such as the distributed stiffness properties). Also, it should be noted that the wing is not exactly cantilevered at the root, as was assumed for the ComboWing analysis. Instead, as seen in Fig. 4, it extends from a 6·55 in spanwise portion named the "Rigid Section" which is supported on two hinge pins. The Rigid Section is locked against Shearflexing and is significantly stiffer in bending and twisting so as to give a reasonable approximation to a cantilever support.

As a construction detail, the surface of the Shearflexing portion of the wing is free to slide over the Rigid Section. Therefore, the Rigid Section does not constrain the Shearflexing action of the rest of the wing, other than sharing the continuous front spar.

Finally, a small strain gauge was attached to the spar near the flapping axis and calibrated to measure the bending moment. For the test conditions, the non-flapping value was 6·22 ftlb which compares with the ComboWing-predicted value of 4·19 ftlb. When these are used with their corresponding lift values to calculate the spanwise lift centre locations (measured from the flapping axis), one obtains that the experimental value is 17·81 in and the theoretical value is 10·92 in. This is a very significant discrepancy which may be due to the closeness of the wingtip to the windtunnel floor (2 in). However, it is more likely to be due to a lift drop off caused by the plate's less than perfect aerodynamic image plane. This notion would seem to be confirmed by the measured lift values being consistently somewhat less than the calculated values.

By way of another check on this, the ComboWing-predicted static twist distribution was incorporated into a lifting line analysis which gave a flapping axis bending moment of 4·75 ftlb and a lift of 4·44 lb, resulting in a spanwise lift centre location of 12·84 in. Although this is closer to the experimental values, it is still much closer to the ComboWing results. Again, this appears to support the notion of an image plane deficiency, giving the conclusion that the experimentally measured performance is conservative.

CONCLUSION

This article has presented a method by which one may predict the flight performance of aeroelastically responding flapping wings. That is, a flapping action is imposed on the elastic axis, and the consequent aerodynamic and inertial-reaction loads give a steady state and time varying bending and twisting response. These motions are then used, in aerodynamic equations, to calculate the performance of the wing.

A major assumption is the strip theory modelling for each segment's aerodynamic behaviour. Moreover, the aeroelastic response calculations require linear, attached flow, aerodynamic equations. However, the subsequent performance calculations allow separated flow effects; the discrepancy between the two aerodynamic models is justified by the ultimate design goal of minimal, localised, separation on a candidate wing resulting from this analysis.

Systematic numerical studies identified important design guidelines for efficient ornithopter wings; and these were followed during the development of a wing with specific performance capabilities for a research model ornithopter. A special feature of this wing is a means by which it may have torsional compliance along with an efficient double-surface aerofoil.

The resulting wing was windtunnel tested with a specially designed flapping rig, with the results comparing very favourably with the predicted performance. Limitations of the test setup were the aerodynamic image plane required where the wing entered the test section and the closeness of the wing spanning the test section. However, since the primary purpose of these tests was to evaluate the suitability of this particular wing for incorporation on the ornithopter, the close clearances had to be tolerated and judgement made concerning the veracity of the results. Overall, it was felt that the experiments gave a favourable validation of the ComboWing design analysis, and that the candidate wing had sufficient performance to achieve successful flight with the ornithopter. In the event this proved to be true, as will be discussed in a subsequent article.

Finally, this development has shown the feasibility of an efficient, practical, ornithopter wing which has a constant semispan simple harmonic root flapping, and pitching which is due solely to aeroelastic response. That is, with an efficient double-surface aerofoil (made possible by the Shearflex action), the semispan can stay constant during upstroke and downstroke. Also, no mechanical articulation is necessary to provide the pitching motion, provided the wing is aeroelastically tailored. Further, with appropriate use of composite materials the resulting wing may be light and aerodynamically clean, yet much stronger than the maximum imposed loads.

ACKNOWLEDGEMENTS

This research was partially supported by an Operating Grant from the Natural Sciences and Engineering Research Council of Canada. Also, this could not have been accomplished without the skilled efforts of University of Toronto research engineers William McKinney and Henry Kwok. Further, this work benefited greatly from the careful study and helpful suggestions of J.M. Harris, Principal Research Engineer at Battelle Memorial Institute and the author's partner in the ornithopter project, who also produced Figs 6 and 9.

REFERENCES

1. GIBBS-SMITH, C.H. The Eighteen Seventies and Eighties, *A History of Flying*, B.T. Batsford, London, 1953, p 172.
2. ARCHER, R.D., SAPUPPO, J. and BETTERIDGE, D.S. Propulsion characteristics of flapping wings, *Aeronaut J*, September 1979, **83**,pp 355-371.
3. RAYNER, J. Vertebrate flapping flight mechanics and aerodynamics, and the evolution of flight in bats, *Biona-report 5*, Gustav Fischer, Stuttgart, 1986, pp 27-74.
4. BROOKS, A.N., MACCREADY, P.B., LISSAMAN, P.B.S. and MORGAN, W.R. Development of a wing-flapping flying replica of the largest Pterosaur, AIAA Paper No. 85-1446, 1985.
5. DELAURIER, J.D. An aerodynamic model for flapping-wing flight, *Aeronaut J*, April 1993, **97**, (964), pp 125-130.
6. DELAURIER, J.D. An experimental study of low-speed single-surface airfoils with faired leading edges, *Low Reynolds Number Aerodynamics*, Proceedings of the Conference, Notre Dame, Indiana, Springer-Verlag, Berlin, 1989, pp 161-173.

APPENDIX

Geometrical properties

$\Lambda = 15{\cdot}38°$, $\Gamma_0 = 27{\cdot}26°$, $AR = 9{\cdot}4$

Station number	$\bar{\theta}_{wash}$ deg	c in	y in	Δy in
1	3·62	11·0	2·0	4·0
2	3·59	11·0	6·0	4·0
3	3·56	11·0	10·0	4·0
4	3·52	11·0	14·0	4·0
5	3·48	11·0	18·0	4·0
6	3·39	10·45	22·0	4·0
7	3·15	9·35	26·0	4·0
8	2·60	8·25	30·0	4·0
9	1·89	7·15	34·0	4·0
10	1·00	6·05	38·0	4·0
11	1·15	5·28	41·56	1·56

Elastic properties

Station number	e in	EI lbft^2	$(GJ)_{spar}$ lbft^2/rad	$(GJ)_{f+r}$ lbft^2/rad
1	0·9288	118·29	11·04	3·734
2	0·9288	118·29	11·04	3·734
3	0·9288	118·29	11·04	3·734
4	0·9288	118·29	11·04	3·734
5	0·9288	118·29	11·04	3·734
6	0·5772	28·389	2·65	3·202
7	0·4992	18·319	1·71	2·293
8	0·4368	12·304	1·148	1·575
9	0·378	8·008	0·747	1·026
10	0·3312	5·349	0·499	0·621
11	–0·7452	1	0·5	0

Inertial properties

Station number	x_s in	m_{spar} slug	m_{f+r} slug	i_{spar} slugft^2	i_{f+r} slugft^2
1	0·75	0·000571	0·0011455	$5·9 \times 10^{-7}$	$9·09 \times 10^{-5}$
2	0·75	0·000571	0·000544	$5·9 \times 10^{-7}$	$4·79 \times 10^{-5}$
3	0·75	0·000571	0·000544	$5·9 \times 10^{-7}$	$4·79 \times 10^{-5}$
4	0·75	0·000571	0·000544	$5·9 \times 10^{-7}$	$4·79 \times 10^{-5}$
5	0·75	0·000571	0·000544	$5·9 \times 10^{-7}$	$4·79 \times 10^{-5}$
6	0·4656	0·000355	0·00052	$2·1 \times 10^{-7}$	$4·17 \times 10^{-5}$
7	0·4032	0·000307	0·000473	$1·4 \times 10^{-7}$	$3·11 \times 10^{-5}$
8	0·3528	0·000269	0·000425	$9·0 \times 10^{-8}$	$2·27 \times 10^{-5}$
9	0·306	0·000233	0·000378	$6·0 \times 10^{-8}$	$1·52 \times 10^{-5}$
10	0·2676	0·000203	0·0006525	$4·0 \times 10^{-8}$	$1·72 \times 10^{-5}$
11	1·834	0·0002	0	$2·3 \times 10^{-6}$	0

Aerodynamic properties

Station number	C_{mac}	a_0 deg	$(a_{stall})_{max}$ deg	$(a_{stall})_{min}$ deg	c_{df}	η_s
1	–0.175	5.33	9.00	–9.00	0.012	0.915
2	–0.175	5.33	9.00	–9.00	0.012	0.915
3	–0.175	5.33	9.00	–9.00	0.012	0.915
4	–0.175	5.33	9.00	–9.00	0.012	0.915
5	–0.175	5.33	9.00	–9.00	0.012	0.915
–0.1575	4.79	9.00	–9.00	0.012	0.914	
–0.1225	3.73	9.00	–9.00	0.012	0.911	
–0.0875	2.66	9.00	–9.00	0.012	0.908	
–0.0525	1.60	9.00	–9.00	0.012	0.905	
–0.0175	0.53	9.00	–9.00	0.012	0.902	
0	0	9.00	–9.00	0.012	0	